NOISE MITIGATION USING SONIC CRYSTAL SCATTERERS COMPOSED OF POROUS CONCRETE WITH RUBBER AND CORK INCLUSIONS

N. Herrera-Leon[1], P. Amado-Mendes[1], L. Godinho[1]

[1] *ISISE, ARISE, Department of Civil Engineering, University of Coimbra, Portugal*

Abstract

Sonic Crystals offer a promising alternative to traditional noise barriers through the creation of spectral bandgaps. However, the performance of rigid scatterers is often limited by narrow attenuation zones. This study investigates the enhancement of SC barriers by utilizing a novel porous concrete matrix modified with recycled rubber shreds or cork powder.

Initially, the acoustic properties of the mixtures were characterized via impedance tube measurements, revealing that rubber additives shift the absorption peak toward higher frequencies, while cork powder significantly broadens the absorption bandwidth. These findings were then applied to a case study of a modular SC barrier. Numerical simulations performed after laboratory measurements of the new mixtures, from which equivalent fluid parameters were obtained, demonstrate that scatterers composed of modified porous concrete provide a synergistic effect: the periodic arrangement maintains Bragg interference, while the intrinsic material absorption complements the insertion loss spectrum. The results indicate that cork-modified scatterers are particularly effective for broadband urban noise, while rubber-modified composites allow for targeted attenuation. This research highlights the potential of functionalized cement-based composites as high-performance, sustainable noise control structures.

Keywords: *porous concrete, sonic crystal, noise barrier, acoustic absorption*

1. Introduction

Noise in urban environments is an increasing problem, with major sources including road traffic, construction, and aircraft. Conventional mitigation methods rely on concrete, metal, or glass barriers, which mainly reflect sound rather than dissipate it. In many applications, sound-absorbing materials are preferable. Common absorbers are fibrous materials (e.g., melamine and rockwool), but they require additional protection for outdoor use.

Porous concrete (PC) is a promising sound-absorbing construction material. It is produced by modifying the aggregate composition to create an interconnected pore network [1]. As sound propagates through these pores, part of its energy is dissipated as heat and structural vibrations [2]. PC is widely used in pavements and highway noise barriers.

Modifying the concrete mix with alternative aggregates is a common strategy to improve its performance. Kim and Lee [3] investigated expanded shale aggregates and found that higher porosity and better-connected pore pathways increase sound absorption through enhanced viscous and thermal losses. Park et al. [4] showed that recycled crushed cement waste alters pore geometry and airflow resistivity, shifting the frequency range of maximum absorption. Overall, these studies demonstrate that controlling void ratio and aggregate selection enables porous concrete to achieve improved acoustic performance while maintaining structural viability.

A key advantage of PC is its compatibility with recycled and natural aggregates. Holmes et al. [5] replaced part of the fine aggregate with crumb rubber from recycled tires, showing that elastic inclusions modify pore structure and improve acoustic performance with limited structural compromise. Similarly, Novais et al. [6] investigated cork-based alkali-activated fly ash composites and reported significant improvements in noise reduction, although mainly for mixtures containing at least 60% cork.

This work investigates the acoustic performance of porous concrete made with expanded clay as the base aggregate and modified with cork or rubber particles. Several mixtures were prepared by replacing portions

Corresponding author: *uc2023166693@student.uc.pt.*

of expanded clay with these aggregates and by increasing the cement content. The absorption coefficient (α) was measured with an impedance tube following ISO 10534 [7], the open porosity (ϕ) using the pressure/mass method [8], and the airflow resistivity (σ) following ISO 9053 [9]. The measured absorption curves were then used to estimate the remaining equivalent fluid parameters, tortuosity (τ_∞) and pore size ($\bar{s}$), through optimization of a transfer matrix method (TMM) model. Finally, the resulting material properties were implemented in a 2D FEM simulation of a sonic crystal (SC) to evaluate the acoustic benefits of the modified aggregates.

2. Materials and experimental methods

2.1. Concrete mix proportions

The original PC mixture was characterized by M. Pereira et al. in [10]. For this study, we are taking what the authors in the study called Mix 2 with an aggregate grain size of 0 to 2 mm. Originally, M. Pereira defined the recipe in mass proportions. To directly create the mixture, the weight proportions are useful. However, to replace the original aggregate (expanded clay) volume proportions are more appropriate. The used base PC composition in volume proportion is the following:

Table 1: A/C/W proportions (%) in volume of the produced porous concrete samples taken from [10].

Granular mixture	Exp. clay-A (%)	Cement-C (%)	Water-W (%)
Mixture 2 0–2 (mm)	69.18	18.59	12.23

For the mixtures analyzed in this work, 50% of the aggregate volume proportion was changed for either cork (K) or rubber (B). After initial trials, it was observed that, especially when using cork, the structural integrity of the samples was insufficient for testing. Consequently, three sets of samples were created for each new aggregate, increasing the amount of cement (C) by 0.1 kg. The following table describes the density and grain size of the new aggregates.

Table 2: Measured density and grain size from the supplier of the used cork and rubber shreds.

Aggregate	Density (kg/m^3)	Grain size (mm)
Cork (K)	98.51	Powder
Rubber (B)	494.37	0 - 2

Having defined the proportions of all the components, the final values for the used mixtures in weight are:

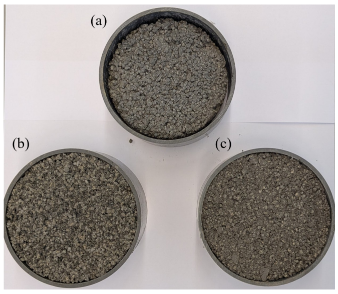

Figure 1: Example of the created samples (a) Pure porous concrete (PC). (b) PC mixed with rubber (B). (c) PC mixed with cork (K).

Table 3: PC mixed with cork (K) weight values (kg) to create 1 kg of mixture

Material	1C	2C	3C
A	0.26	0.26	0.26
K	0.06	0.06	0.06
W	0.23	0.23	0.23
C	0.45	0.55	0.65

Table 4: PC mixed with rubber (B) weight values (kg) to create 1 kg of mixture

Material	1C	2C	3C
A	0.21	0.21	0.21
K	0.25	0.25	0.25
W	0.18	0.18	0.18
C	0.36	0.46	0.56

Using these mixtures, three cylindrical specimens were cast for each combination of cement content and material type to be used in posterior experimental testing. The samples have an internal diameter of 10 cm and a height of 5 cm.

2.2. Direct experimental characterization

Once the samples were created, they needed at least two weeks to fully cure and dry. After that time, they can be experimentally tested. To numerically model absorbing materials, equivalent fluid models are used. They mathematically describe the material through a series of parameters. For the case of this study, the JCA model was selected. This model is widely used to describe multiple types of absorbing materials.
The original PC mixture has the following properties to model it:
$\bar{s}$ is important in this work because, with it, the viscous (Λ) and thermal (Λ') characteristic lengths through the equations developed in [11].

$$\Lambda = \bar{s}e^{-5/2(\sigma_p \log 2)^2}, \quad (1)$$

$$\Lambda' = \bar{s}e^{3/2(\sigma_p \log 2)^2}. \quad (2)$$

For the new PC compositions, it is necessary to obtain the same properties as the original PC mixture. σ

Table 5: Material properties for the pure porous concrete mixture.

Parameter	Value
σ (N s/m^4)	3896.06
ϕ	0.46
τ_∞	1.89
σ_p	0.25
$\bar{s}$ (mm)	0.35

Figure 2: Open porosity (ϕ) testing machine with sample.

and ϕ can be directly measured using specialized laboratory equipment. τ_∞ and $\bar{s}$ will be obtained through an optimization adjusting the experimental α curve with one obtained numerically using the JCA model. The optimization procedure is better described in Sec. 3.

2.2.1. Porosity

The work developed by Salissou and Panneton [8] describes a gas porosimeter test method that determines the open porosity of a solid by performing four precise mass measurements at two static pressures, and applying the perfect gas law to interpret the results. The procedure uses a rigid airtight cylinder that is alternately evacuated and pressurized with a gas (i. e., air, argon). First, the empty chamber is weighed at low pressure and high pressure; then the sample is inserted, and the same two measurements are repeated. Because the mass of gas inside the chamber changes with pressure and with the volume displaced by the solid phase of the sample, comparing these four masses allows the researchers to compute the solid phase volume V_s. Once the latter is known, the open porosity follows directly from $\phi = V_s/V_{total}$.

2.2.2. Airflow resistivity

The method used to obtain σ is described in the ISO 9053-1:2026 standard [9]. The standard defines the laboratory procedure for measuring the static airflow resistivity of open-porous materials. The test operates by forcing a steady, unidirectional, laminar airflow through a specimen of known thickness (d) and cross-sectional area (A) while measuring the resulting static pressure drop (Δp) across its faces. By dividing this pressure differential by the linear airflow velocity (v), the method determines the material's specific airflow resistance ($R_s = \Delta p/v$). Dividing R_s by the sample thickness yields the static airflow resistivity

Figure 3: Airflow resistivity (σ) testing machine with sample.

($\sigma = R_s/d$), expressed in Pa $\cdot$ s/m^2, which quantifies the resistance the material's internal pore network poses to moving air per unit depth.

2.2.3. Absorption coefficient

α was experimentally obtained by following the ISO 10534-2 standard [7]. The measurements were performed using the transfer function method. This method computes the ratio of complex pressures registered by the two microphones; by doing this, it is possible to determine the change between incident and reflected waves. The experimental setup will measure the complex reflection coefficient R. The sound absorption coefficient, α, is therefore calculated by: $\alpha = 1 - |R|^2$

3. JCA parameter optimization

3.1. Inverse optimization

To fully characterize the acoustic behavior of the material using the JCA equivalent fluid model, an inverse characterization method is employed. While macroscopic properties such as σ and ϕ were measured experimentally, non-acoustic parameters like τ_∞ and the characteristic lengths are highly complex to determine directly.

This problem is framed as a bounded, non-linear optimization routine. The objective is to find the optimal vector of state variables, $\mathbf{x} = [\tau_\infty, \bar{s}, \sigma, \phi]$, that minimizes the root-mean-square error (RMSE) between the analytically predicted sound absorption coefficient, α_{model}, and the experimentally measured values, α_{exp}, obtained via the impedance tube method. The optimization problem is defined as:

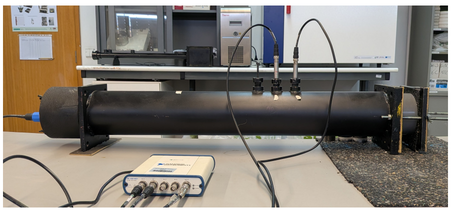

Figure 4: Impedance tube used to experimentally measure the sound absorption coefficient (α) with sample on the right side.

$$\min_{\mathbf{x}} F(\mathbf{x}) = \sqrt{\frac{1}{N}\sum_{i=1}^{N}\left(\alpha_{\text{model}}(f_i,\mathbf{x}) - \alpha_{\text{exp}}(f_i)\right)^2} \quad (3)$$

subject to the boundary constraints:

$$\mathbf{x}_{lb} \leq \mathbf{x} \leq \mathbf{x}_{ub}, \quad (4)$$

Where N is the total number of frequency points evaluated. To account for instrumental uncertainties in the macroscopic measurements, σ and ϕ are not rigidly fixed; rather, they are bounded by their measured nominal values plus or minus the known tolerance of the testing equipment, allowing the algorithm sufficient flexibility to converge on a physically accurate global minimum.

The optimization is implemented using a Sequential Quadratic Programming (SQP) algorithm. To ensure the reliability of the fit, the experimental dataset is strictly filtered to the 200 Hz to 2000 Hz range, corresponding to the valid plane-wave frequency limits of the impedance tube apparatus and minimizing the influence of low-frequency phase errors. During each iteration, the algorithm updates the state variables and calculates the frequency-dependent dynamic mass density and bulk modulus. For this specific implementation, the viscous and thermal characteristic lengths are calculated using Eqs. 1 and 2.

The surface impedance (Z) is then derived from the equivalent fluid properties, and the theoretical absorption coefficient is computed at each target frequency point f_i. The SQP algorithm evaluates the gradient of the objective function, iteratively refining the parameter set $\mathbf{x}$ until the step size or the change in the RMSE falls below the convergence tolerance, yielding the finalized material properties.

3.2. Results

Fig. 5 illustrates the different measured α of the pure PC mixture, the PC mixtures with K and B, and the calculated α curve of the new mixtures after the optimization routine. Overall the agreement between the calculated and experimental curves is good. For 5 of the 6 cases the peak matches in frequency and amplitude. Fig. 5 (b) is the only mixture where the used base optimization was not enough to approximate the macroscopic parameters to a point where the material is correctly characterized. For this case further refinement is necessary. Furthermore, all the cases show a shift to low frequencies in the peak absorption and a general widening of the curve. This effect is cause by the reduction of the larger interconnected voids in the concrete matrix. The rubber or cork bridge those bigger pores increasing the porosity and airflow resistivity. A moderate increase in σ increases the damping, which broadens the absorption curve and shifts the peak absorption toward lower frequencies.

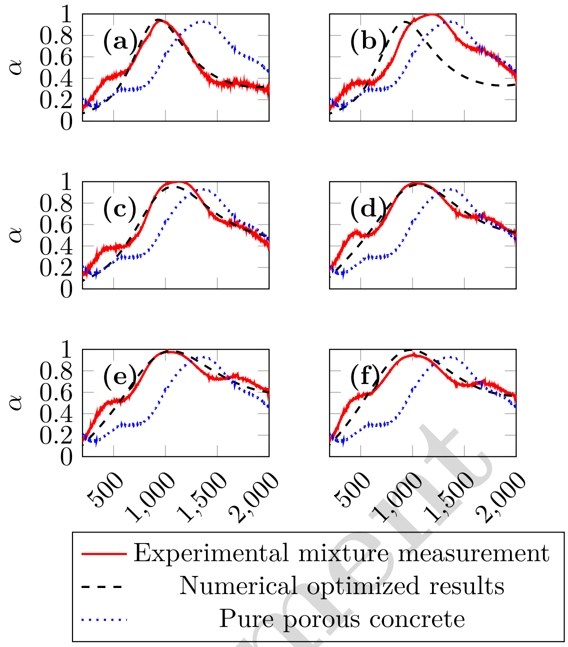

Figure 5: Comparison between experimentally measured absorption coefficient (α), calculated α curve of the new mixtures after the optimization routine, and measured α of the pure PC mixture for: (a) 1C-B, (b) 2C-B, (c) 3C-B, (c) 3C-B, (d) 1C-K, (e) 2C-K, (f) 3C-K.

Tab. 6 summarizes the final values that characterize each mixture.

Table 6: Optimized material properties for the different porous concrete mixtures.

Mixture	σ	ϕ	τ_∞	$\bar{s}$
1C-B	4976.67	0.588	4.605	0.43
2C-B	3624.44	0.634	2.699	0.25
3C-B	3581.11	0.641	2.906	0.27
1C-K	9493.33	0.717	2.954	0.34
2C-K	8725.22	0.729	2.587	0.23
3C-K	10950	0.716	3.027	0.25

4. Application to sonic crystal noise barrier

4.1. Numerical setup

To test an application of the newly characterized mixtures, the authors developed a case study with a sonic crystal with a 2 cm layer of PC as an external absorbing layer. The external (d_1) and internal (d_2) diameter of the SC are 12 and 8 cm, respectively. The lattice constant (a) is 17 cm, which means that the peak of attenuation will theoretically occur at 1000 Hz. Fig. 6 (a) shows the geometric parameters of the used geometry. Fig. 6 (b) illustrates the used mesh. The used frequency range goes from 50 to 2000 Hz. The maximum element size of the mesh is a sixth of the wavelength of the maximum study frequency.
The interest parameter to evaluate the SC is insertion loss (IL), which is defined as:

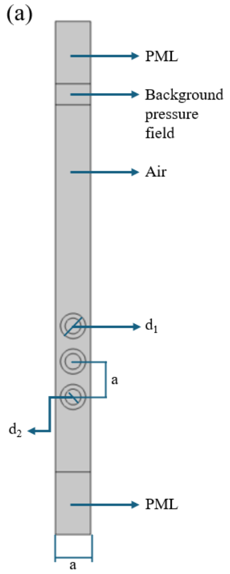

Figure 6: Used FEM model for the SC noise barrier evaluation. (a) Domain definition and geometric parameters. (b) Used mesh for the system.

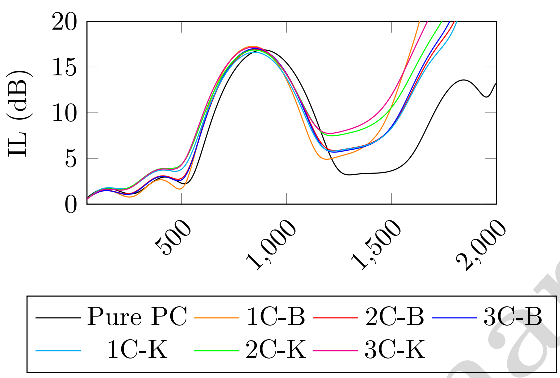

Figure 7: IL results per microphone for the absorbing layer configuration SC.

$$IL = SPL_{\text{without}} - SPL_{\text{with}} \quad [\text{dB}] \tag{5}$$

where SPL_{without} corresponds to the sound pressure level (SPL) values without the SC, and SPL_{with} are the SPL values when the SC is applied.

4.2. Acoustic performance evaluation

Fig. 7 illustrates the IL results when updating the porous layer properties to match the optimized parameters summarized in Tab. 6. As expected, the reference PC mixture exhibits the lowest acoustic performance across all evaluated cases. In the low-frequency regime, only the cork-based mixtures enhance the performance of the sonic crystal (SC), whereas the rubber-based mixtures yield negligible impact below the Bragg band gap. Because cork possesses intragranular porosity, its inclusion creates a dual-porosity matrix. This dual-porosity mechanism enhances low-frequency sound absorption within the cementitious matrix, an effect absent in the rubber mixtures due to rubber's predominantly reflective nature.

Both additive types induce a slight shift of the primary band gap toward lower frequencies. The heightened absorption within the porous layer enhances destructive interference, further attenuating the acoustic energy associated with the Bragg scattering of the SC. The distinction between the two material types becomes most pronounced above the band gap. Here, the rubber mixtures increase the IL by approximately 3 dB or more between 1200 Hz and 1500 Hz, regardless of the cement content. While the cork mixture 1C-K exhibits a trend similar to the rubber samples in this range, the remaining two cork compositions yield substantial gains, elevating the IL by 5 dB or more. Furthermore, the absorbing layer completely suppresses the second Bragg band gap of the SC, leading to a significant overall IL enhancement at higher frequencies.

5. Conclusion

This study successfully characterized and modeled the acoustic performance of novel porous concrete (PC) composites modified with recycled rubber shreds and cork powder. By pairing direct laboratory measurements with a JCA based inverse optimization routine, the equivalent fluid parameters of the new mixtures were accurately determined. The structural integration of these low-density, elastic inclusions modified the internal pore network, leading to a moderate increase σ and ϕ. This physical shift successfully broadened the overall sound absorption curves and shifted the peak acoustic absorption toward lower frequencies compared to conventional porous concrete.

When applied as a 2 cm external absorbing layer in a SC noise barrier, both modified composites significantly outperformed the reference porous concrete. Due to the intragranular porosity of cork, which creates a dual porosity matrix, its mixtures enhanced acoustic performance in the low-frequency regime below the Bragg band gap. Above the main band gap, the cork composites achieved substantial IL gains of 5 dB or more, while the rubber composites provided a targeted IL increase of approximately 3 dB or more between 1200 Hz and 1500 Hz. Furthermore, both additives shifted the primary band gap toward lower frequencies and suppressed the secondary Bragg band gap of the SC.

Ultimately, cement composites with sustainable, recycled materials provide a highly viable, eco-friendly design pathway for high-performance urban noise control structures. The combination of periodic Bragg scattering and localized material absorption offers a powerful synergistic mechanism for broadband noise mitigation.

6. Acknowledgments

The European Commission is gratefully acknowledged for their support of the Horizon Europe DN METAVISION project (GA 101072415). Views and opinions expressed are, however, those of the authors only and do not necessarily reflect those of the European Union. The European Union cannot be held responsible for them.

This work was supported by the Fundação para a Ciência e a Tecnologia (FCT) through national funds and by the Fundo Europeu de Desenvolvimento Regional (FEDER) through the Thematic Programme Innovation and Digital Transition (COMPETE 2030), under Portugal 2030, and by the European Union, within the framework of Project No. 14677 — COMPETE2030-FEDER-00917500 (https://doi.org/10.54499/2023.16029.ICDT). This work was also funded by national funds through FCT – Fundação para a Ciência e a Tecnologia, I.P., under the project 2024.17219.PEX - https://doi.org/10.54499/2024.17219.PEX.

This work was also supported by FCT/MCTES under the R&D Unit Institute for Sustainability and Innovation in Structural Engineering (ISISE), under the references UID/4029/2025 (https://doi.org/10.54499/UID/04029/2025) and UID/PRR/04029/2025 (https://doi.org/10.54499/UID/PRR/04029/2025), and under the Associate Laboratory Advanced Production and Intelligent Systems ARISE under reference LA/P/0112/2020 (https://doi.org/10.54499/LA/P/0112/2020).

References

[1] N. Neithalath, J. Weiss, and J. Olek, "Characterizing enhanced porosity concrete using electrical impedance to predict acoustic and hydraulic performance," *Cement and Concrete Research*, vol. 36, no. 11, pp. 2074–2085, 2006, ISSN: 0008-8846. DOI: https://doi.org/10.1016/j.cemconres.2006.09.001. [Online]. Available: https://www.sciencedirect.com/science/article/pii/S0008884606002122.

[2] N. Takao, J. Xuemei, M. Isao, and S. Shigeo, "The influence of the sound absorption ability by the aggregate size and void ratio of porous concrete about sound absorption characteristics of porous concrete," *Proc. Jpn. Constr. Inst*, vol. 23, pp. 163–168, 2001.

[3] H. Kim and H. Lee, "Influence of cement flow and aggregate type on the mechanical and acoustic characteristics of porous concrete," *Applied Acoustics*, vol. 71, no. 7, pp. 607–615, 2010, ISSN: 0003-682X. DOI: https://doi.org/10.1016/j.apacoust.2010.02.001. [Online]. Available: https://www.sciencedirect.com/science/article/pii/S0003682X1000037X.

[4] S. B. Park, D. S. Seo, and J. Lee, "Studies on the sound absorption characteristics of porous concrete based on the content of recycled aggregate and target void ratio," *Cement and Concrete Research*, vol. 35, no. 9, pp. 1846–1854, 2005, ISSN: 0008-8846. DOI: https://doi.org/10.1016/j.cemconres.2004.12.009. [Online]. Available: https://www.sciencedirect.com/science/article/pii/S0008884605000220.

[5] N. Holmes, A. Browne, and C. Montague, "Acoustic properties of concrete panels with crumb rubber as a fine aggregate replacement," *Construction and Building Materials*, vol. 73, pp. 195–204, 2014, ISSN: 0950-0618. DOI: https://doi.org/10.1016/j.conbuildmat.2014.09.107. [Online]. Available: https://www.sciencedirect.com/science/article/pii/S0950061814011234.

[6] R. M. Novais et al., "Multifunctional cork – alkali-activated fly ash composites: A sustainable material to enhance buildings' energy and acoustic performance," *Energy and Buildings*, vol. 210, p. 109 739, 2020, ISSN: 0378-7788. DOI: https://doi.org/10.1016/j.enbuild.2019.109739. [Online]. Available: https://www.sciencedirect.com/science/article/pii/S0378778819328531.

[7] *Determination of acoustic properties in impedance tubes. iso 10534-2:2023*, Available at: https://www.iso.org/standard/81294.html, International Organization for Standardization, 2023.

[8] Y. Salissou and R. Panneton, "Pressure/mass method to measure open porosity of porous solids," *Journal of Applied Physics*, vol. 101, no. 12, p. 124 913, Jun. 2007, ISSN: 0021-8979. DOI: 10.1063/1.2749486. eprint: https://pubs.aip.org/aip/jap/article-pdf/doi/10.1063/1.2749486/14998634/124913_1_online.pdf. [Online]. Available: https://doi.org/10.1063/1.2749486.

[9] *Acoustics — determination of airflow resistance — part 1: Static method*, Available at: https://www.iso.org/standard/90718.html, International Organization for Standardization, 2026.

[10] M. Pereira, J. Carbajo, L. Godinho, P. Amado-Mendes, D. Mateus, and J. Ramis, "Acoustic behavior of porous concrete. characterization by experimental and inversion methods.," *Materiales de Construcción*, vol. 69, no. 336, e202, Dec. 2019. DOI: 10.3989/mc.2019.03619. [Online]. Available: https://materconstrucc.revistas.csic.es/index.php/materconstrucc/article/view/2270.

[11] K. V. Horoshenkov, J.-P. Groby, and O. Dazel, "Asymptotic limits of some models for sound propagation in porous media and the assignment of the pore characteristic lengths," *The Journal of the Acoustical Society of America*, vol. 139, no. 5, pp. 2463–2474, May 2016, ISSN: 0001-4966. DOI: 10.1121/1.4947540. [Online]. Available: https://doi.org/10.1121/1.4947540.